Resonance in low-temperature oxidation waves for porous media[*]

A.A. Mailybaev[‡][†]   D. Marchesin[‡]   J. Bruining[§]

May 4, 2012

Abstract

This paper analyzes traveling wave profiles possessing an internal resonance point for a class of systems of partial differential equations describing oxidation and vaporization of liquid fuel in a porous medium when an oxidizer (air) is injected. It is shown that the resonance is characterized by a saddle point of an associated vector field defined on a folded surface in state space. We prove existence and uniqueness of this singularity for an open set of parameters. The singularity yields an extra restriction on wave parameters. This restriction is found explicitly in the physically relevant case of a small ratio of reaction/vaporization rates. We find the general large time asymptotic solutions of the problem as a sequence of waves, and show that resonance waves play a key role in determining these solutions. A numerical example is presented.

1 Introduction

The mathematical theory of combustion [25] is an exciting area of applied mathematics encompassing a vast number of problems, techniques and phenomena. Problems of combustion in one-dimensional space are of special interest. They allow a detailed analytical study of the combustion process; filtration combustion in a porous medium is a good example, e.g., [21, 4]. Sustained combustion is the simplest combustion mode that one is able to describe analytically, providing the basis for studying more complicated (periodic or chaotic) types of solutions, e.g., [16, 2]. These solutions form an important contribution to understanding reactive transport processes in porous media with applications to groundwater flow and enhanced oil recovery. .

This paper presents a nonlinear wave solution originating from the problem of combustion of a liquid fuel filtrating in one-dimensional porous medium when an oxidizer (air) is injected. Such a combustion process can be found in low-temperature oxidation (LTO) of low-viscosity oil, a prospective technique for enhanced oil recovery [24], or as one aspect the high-pressure air injection [8]. The mathematical model is given by a system of multi-phase flow equations with additional terms describing reaction and vaporization rates, and an energy balance equation.

Despite similarities to problems in multi-phase flows [20, 10, 3], filtration combustion [18, 21], drying theory [22] etc., the problem provides a novel type of nonlinear waves with interesting structure properties. On the one hand, the analysis of the internal wave structure (the reaction zone) is necessary in order to obtain macroscopic parameters of the wave. On the other hand,

[†]Institute of Mechanics, Moscow State University, Michurinsky pr. 1, 119192 Moscow, Russia (mailybaev@imec.msu.ru).

[‡]Instituto Nacional de Matemática Pura e Aplicada, Estrada Dona Castorina 110, 22460-320 Rio de Janeiro, Brazil (marchesi@impa.br).

[§]TU Delft, Civil Engineering and Geosciences, Stevinweg 1, 2628 CE Delft, The Netherlands (J.Bruining@tudelft.nl).

the determining equations appear to be independent of the particular form of the rate terms, as soon as one of the processes is much faster (in our applications, vaporization is usually much faster than combustion). The resulting combustion wave is characterized by a singularity of the wave profile, which can be described and analyzed as a saddle of a vector field defined on a folded surface in the state space. This singularity is related to a resonance in which the wave speed coincides with a characteristic speed at an isolated internal point of the wave profile. The resulting wave solution can be characterized as a nonclassical traveling wave [12, 15], with a singular internal structure. Traveling waves profiles with a similar singularity were encountered in detonation problems, see [23, 6, 19, 11]. The novelty of our paper are rigorous results on the traveling waves, as well as on existence and uniqueness of the wave sequence solutions, obtained by the usage of the large vaporization rate limit.

The paper is organized as follows. Section 2 describes the physical model and presents the dimensionless equations. Section 3 provides the equations to be solved for the combustion wave profile. In Section 4, we first consider a simple choice of parameters, for which the wave profile can be readily analyzed yielding existence and uniqueness theorems. Then these results are extended to the general case. The relevance of resonance is explained in Section 4.5. Section 5 describes waves sequence solutions appearing in the long time asymptotic regime. Section 6 provides a numerical example. We summarize the results in the Conclusion section.

2 Model

We consider flows possessing a combustion front when a gaseous oxidizer (air) is injected into a porous medium, a rock cylinder thermally insulated preventing lateral heat losses, filled with liquid fuel. We consider hydrocarbon fuels such as gasoline or light oil. When oxygen reacts with hydrocarbons at low temperatures, a series of reactions occur that convert a part of hydrocarbons into oxygenated hydrocarbons (ketones, alcohols, aldehydes, etc.) and gaseous products (H_2O, CO_2, etc.). This low temperature oxidation (LTO) reaction is modelled as

$$\text{(hydrocarbons)} + O_2 \rightarrow \text{(oxygenated hydrocarbons)} + \nu_g \text{ (gaseous products)}, \qquad (2.1)$$

i.e., one mole of oxygen reacts with a certain amount of hydrocarbons generating oxygenated hydrocarbons together with ν_g moles of gaseous products. The LTO reaction, in principle, could occur in both liquid and gaseous phases. In our applications the porous rock has small pores, which reduces the free radical concentration in the gas phase, leading to negligible gas reaction rates, see [14] for more details. We neglect water that may by present initially or condenses from steam in the reaction products.

LTO leads to a combination of products, such as gaseous combustion products, small hydrocarbons and oxygenated hydrocarbons, which have a somewhat higher boiling point than the original hydrocarbons. To avoid complex modeling we assume that the combustion products have added oxygen atoms to the original hydrocarbon, but retain the same other properties (density, viscosity etc.) In other words, we disregard the difference in physical properties between oxygenated and original hydrocarbons and consider a single liquid fuel pseudo-component. In the case of oil this assumption implies, in particular, that so little heavy hydrocarbons will be in the original oil that they will evaporate before high temperature oxidation can occur [13].

We study motion in one space direction x. The porous volume contains liquid fuel and gas moving in the positive x-direction. The fuel acts as a single pseudo-component liquid with molar weight M [kg/mole] and saturation (i.e., the occupied fractions of pore volume) s. In our notations, we will use no subscript for quantities related to the liquid fuel phase, and the subscript g for quantities in the gaseous phase. The saturation of gas is, therefore, equal to $s_g = 1 - s$. In the gaseous phase, we distinguish between the molar fraction of gaseous fuel X

and of oxygen Y. The remaining components with fraction $Z = 1 - X - Y$ consist of reaction products and inert components of the injected gas.

Neglecting parabolic terms originating from gas mass diffusion and capillarity effects, the mass balance equations for liquid fuel, total gas, and gas components (gaseous fuel and oxygen) are

$$\frac{\partial}{\partial t}\varphi\rho s + \frac{\partial}{\partial x}\rho u f = -W_v, \tag{2.2}$$

$$\frac{\partial}{\partial t}\varphi\rho_g s_g + \frac{\partial}{\partial x}\rho_g u f_g = (\nu_g - 1)W_r + W_v, \tag{2.3}$$

$$\frac{\partial}{\partial t}\varphi\rho_g X s_g + \frac{\partial}{\partial x}\rho_g u X f_g = W_v, \tag{2.4}$$

$$\frac{\partial}{\partial t}\varphi\rho_g Y s_g + \frac{\partial}{\partial x}\rho_g u Y f_g = -W_r. \tag{2.5}$$

The balance law for the gaseous components included in the fraction $Z = 1 - X - Y$ can be recovered by subtracting (2.4), (2.5) from (2.3). In the equations, W_v [mole/m³s] is the vaporization rate of liquid fuel and W_r [mole/m³s] is the consumption rate of oxygen in the LTO reaction; according to (2.1) $\nu_g W_r$ is the generation rate of gaseous products from the oxidation. Also, φ is the rock porosity, ρ [mole/m³] is the molar density of liquid fuel (the conventional mass density [kg/m³] is, therefore, $M\rho$), u [m/s] is the total seepage (Darcy) velocity, and we use the ideal gas law to define

$$\rho_g = P_{tot}/RT, \tag{2.6}$$

the molar density of gas at the prevailing pressure P_{tot} [Pa] and temperature T [K]. The pressure drop due to flow is assumed to be small compared to the prevailing pressure, so we take $P_{tot} = const$ in (2.6). The fuel and gas fractional flow functions depend on s and T and have the form

$$f = \frac{k/\mu}{k/\mu + k_g/\mu_g}, \quad f_g = 1 - f, \tag{2.7}$$

with viscosities $\mu(T)$, $\mu_g(T)$ [kg/m s] of the liquid fuel and gas, and with relative permeability functions $k(s)$, $k_g(s)$.

Assuming that the temperature of solid rock, fuel and gas are equal, neglecting transversal heat losses and longitudinal heat conduction, we write the heat transport equation as

$$\frac{\partial}{\partial t}\left(C_m + \varphi c\rho s + \varphi c_g \rho_g s_g\right)\Delta T + \frac{\partial}{\partial x}(c\rho f + c_g \rho_g f_g)u\Delta T = Q_r W_r - Q_v W_v. \tag{2.8}$$

Here $\Delta T = T - T_{res}$ with reservoir temperature T_{res}, C_m [J/m³K] is the (constant) heat capacity of the porous rock, c [J/mole K] is the heat capacity of liquid fuel per mole assumed to be a constant, and $c_g \approx 3.5R$ [J/mole K] is the gas heat capacity, ignoring small variations of heat capacity among different gas components. Taking the heat capacities constant is a good approximation that facilitates the analysis. The positive heats (enthalpies) Q_r [J/mole of O_2] and Q_v [J/mole of fuel] correspond to LTO reaction and vaporization of fuel evaluated at the reservoir temperature T_{res}.

The reaction rate W_r depends on T, s, Y. It is positive, but vanishes for $s = 0$ (no fuel) or $Y = 0$ (no oxygen). The vaporization rate W_v depends on T, s, X. It vanishes when the liquid fuel is in thermodynamic equilibrium with the gaseous phase, i.e., either when $X = X_{eq}$, or when $s = 0$ with $X \leq X_{eq}$. When $s > 0$, the derivative $\partial W_v/\partial X < 0$, so that $W_v > 0$ for $X < X_{eq}$. The equilibrium fraction of gaseous fuel is given by the Clausius-Clapeyron relation

$$X_{eq} = \frac{P_{atm}}{P_{tot}}\exp\left(-\frac{Q_v}{R}\left(\frac{1}{T} - \frac{1}{T_n}\right)\right), \tag{2.9}$$

where T_n [K] is the boiling point for fuel at atmospheric pressure P_{atm}. Taking $X_{eq} = 1$ in (2.9), one recovers the actual boiling temperature $T = T_b$ at pressure P_{tot}.

The LTO reaction at the temperatures under consideration is relatively slow, leading to large typical spatial scales. Such scales justify our assumptions of neglecting longitudinal heat conduction, diffusion and capillary effects, which are described by second-order derivative terms with respect to x. Also, the vaporization process is much faster than the LTO reaction. In this case, as we will see later, the specific forms of the reaction and vaporization rates W_r and W_v are not important for determining macroscopic solution parameters; they affect only the width of the LTO wave and its internal structure.

The five equations (2.2)–(2.5), (2.8) constitute a system with dependent variables (s, u, X, Y, T). They are non-dimensionalized by introducing dimensionless dependent and independent variables as ratios of dimensional quantities and reference quantities denoted by an asterisk:

$$\tilde{t} = \frac{u^* t}{\varphi x^*}, \quad \tilde{x} = \frac{x}{x^*}, \quad \tilde{\theta} = \frac{T - T_{res}}{T^*}, \quad \tilde{u} = \frac{u}{u^*}, \tag{2.10}$$

where

$$x^* = \frac{Y_{inj} \rho_g^* u^*}{W_r^*}, \quad \rho_g^* = \frac{P_{tot}}{RT_{res}}, \quad T^* = T_b - T_{res}. \tag{2.11}$$

Also W_r^* is the reference value of the reaction rate, and u^* is the reference seepage velocity specified later. The dimensionless quantities $\tilde{\theta}$ and $\tilde{u}$ describe the temperature (measured from the reservoir condition) and seepage velocity, respectively. The length scale x^* in (2.11) is the ratio between rate of oxygen injection and rate of oxygen consumption in the LTO reaction. It is a reference length of the LTO reaction region. The dimensionless reaction and vaporization rates are $w_r = Y_{inj} W_r / W_r^*$, $w_v = W_v / W_v^*$ with corresponding characteristic rates W_r^*, W_v^* (as has been already mentioned, we will not need to specify these rates in detail).

The dimensionless equations are obtained by using (2.6), (2.10), (2.11) in equations (2.8), (2.2)–(2.5), (2.9) and then omitting the tildes. Constant dimensionless parameters are introduced as

$$\alpha = \frac{\varphi c \rho}{C_m}, \quad \alpha_g = \frac{\varphi c_g \rho_g^*}{C_m}, \quad \beta = \frac{\rho_g^*}{\rho}, \quad \gamma = \frac{\varphi \rho_g^* Q_r}{C_m T^*}, \quad \sigma = \frac{Q_v}{Q_r},$$

$$\theta_v = \frac{Q_v}{RT^*}, \quad \theta_0 = \frac{T_{res}}{T^*}, \quad \varepsilon = \frac{Y_{inj} W_v^*}{W_r^*}. \tag{2.12}$$

Note that the dimensionless parameters are independent of the characteristic velocity u^*. Thus, every solution of our system generates a family of solutions with dimensional variables x and u scaled proportionally to u^*, see (2.10), (2.11).

2.1 Governing system of equations in dimensionless form

The governing system of equations for the energy, fuel, total gas, gaseous fuel and oxygen in dimensionless form (after dropping tildes) is

$$\frac{\partial}{\partial t} (1 + \alpha s + \alpha_g S_g) \theta + \frac{\partial}{\partial x} (\alpha f + \alpha_g F_g) u\theta = \gamma w_r - \frac{\sigma \gamma w_v}{\varepsilon}, \tag{2.13}$$

$$\frac{\partial s}{\partial t} + \frac{\partial}{\partial x} uf = -\frac{\beta w_v}{\varepsilon}, \tag{2.14}$$

$$\frac{\partial S_g}{\partial t} + \frac{\partial}{\partial x} uF_g = (\nu_g - 1)w_r + \frac{w_v}{\varepsilon}, \tag{2.15}$$

$$\frac{\partial}{\partial t} XS_g + \frac{\partial}{\partial x} uXF_g = \frac{w_v}{\varepsilon}, \tag{2.16}$$

$$\frac{\partial}{\partial t} YS_g + \frac{\partial}{\partial x} uYF_g = -w_r, \tag{2.17}$$

with temperature-corrected gas saturation and flow function

$$S_g(s, \theta) = \frac{1 - s}{1 + \theta/\theta_0}, \quad F_g(s, \theta) = \frac{1 - f}{1 + \theta/\theta_0}. \tag{2.18}$$

The dependent variables in system (2.13)–(2.17) are s, X, Y (defined in the interval $[0, 1]$), θ, and u. Properties of the functions $f(s, \theta)$, $w_r(s, Y, \theta)$ and $w_v(s, X, \theta)$ are specified later.

As it is common in applied problems, some of the equations can be rewritten as conservation laws, see, e.g., [9]. Indeed, using w_r and w_v from (2.16), (2.17), the equations (2.13)–(2.15) are written as

$$\frac{\partial}{\partial t} [(1 + \alpha s + \alpha_g S_g) \theta + \gamma(Y + \sigma X)S_g] + \frac{\partial}{\partial x} [(\alpha f + \alpha_g F_g) u\theta + \gamma(Y + \sigma X)uF_g] = 0, \tag{2.19}$$

$$\frac{\partial}{\partial t} (s + \beta XS_g) + \frac{\partial}{\partial x} (uf + \beta XuF_g) = 0, \tag{2.20}$$

$$\frac{\partial}{\partial t} (1 - X + (\nu_g - 1)Y)S_g + \frac{\partial}{\partial x} (1 - X + (\nu_g - 1)Y)uF_g = 0. \tag{2.21}$$

For the equilibrium fraction of gaseous fuel, we have

$$X_{eq}(\theta) = \exp\left(\frac{\theta_v}{\theta_0 + 1} - \frac{\theta_v}{\theta_0 + \theta}\right). \tag{2.22}$$

The liquid fuel and gas viscosities satisfy

$$\frac{d\mu}{d\theta} < 0, \quad \frac{d\mu_g}{d\theta} > 0. \tag{2.23}$$

Under physically reasonable hypotheses on k and k_g, we can assume that $f(s, \theta)$ in (2.7) is a smooth function satisfying the conditions

$$f = \frac{\partial f}{\partial s} = 0 \text{ when } s = 0; \quad f_g = \frac{\partial f_g}{\partial s} = 0 \text{ when } s = 1; \tag{2.24}$$

$$\frac{\partial f}{\partial \theta} > 0, \quad \frac{\partial f}{\partial s} > 0 \text{ when } 0 < s < 1; \tag{2.25}$$

$$\partial^2 f/\partial s^2 > 0 \text{ for } 0 < s < s^I; \quad \partial^2 f/\partial s^2 < 0 \text{ for } s^I < s < 1; \tag{2.26}$$

where $s^I(\theta)$ is the single inflection point of $f(s, \theta)$ as a function of s.

The reaction and vaporization rates $w_r(s, Y, \theta)$, $w_v(s, X, \theta)$ are smooth functions satisfying the conditions

$$w_r = 0 \ \text{ if } \ s = 0 \ \text{ or } \ Y = 0; \quad \text{otherwise } \ w_r > 0; \tag{2.27}$$

$$w_v = 0 \ \text{ if } \ X = X_{eq}(\theta); \quad w_v = 0 \ \text{ if both } \ s = 0 \text{ and } X \le X_{eq}(\theta);$$

$$\partial w_v / \partial X < 0 \ \text{ if } \ s > 0. \tag{2.28}$$

Conditions (2.28) imply that

$$w_v > 0 \ \text{ for } \ s > 0, \ X < X_{eq}(\theta); \quad w_v < 0 \ \text{ for } \ s > 0, \ X > X_{eq}(\theta). \tag{2.29}$$

We also assume

$$0 < \partial w_r / \partial s < \infty, \quad 0 < \partial w_v / \partial s < \infty \quad \text{for} \quad s = 0, \ X = 0, \ Y > 0, \tag{2.30}$$

which implies the regular (linear) decrease of the rates $w_r \to 0$ and $w_v \to 0$ as s tends to zero.

Remark. In many applications, such as petroleum engineering, the function $f = 0$ for $0 \le s \le s_{irr}$ with the irreducible saturation s_{irr}, while conditions analogous to (2.24)–(2.26) are satisfied in the interval $s_{irr} \le s \le 1$. Also, the derivative $\partial w_v / \partial X$ can be discontinuous at $X = X_{eq}(\theta)$, and the limiting behavior of the rates for small s can be different from (2.30). In our analysis, we consider the case $s_{irr} = 0$ and smooth w_v. However, with some modifications of the proofs, the results of the current work can be extended to the general case.

All parameters defined in (2.12) are constant. The ratio between reaction rate and evaporation rate is assumed to be small, i.e.,

$$\varepsilon \ll 1 \tag{2.31}$$

(a typical value of ε is extremely small, e.g., 10^{-5}). For simplicity, we assume that

$$\beta < 1. \tag{2.32}$$

This condition is always satisfied in practical applications, since the gas density ρ_g^* is smaller than the liquid fuel density ρ, see (2.12).

3 Traveling wave equations for the LTO wave

The subject of our study is the LTO wave, where oxygen reacts with fuel. We look for the solution in the form of waves traveling with constant speed $v > 0$. All the variables in these waves depend on a single traveling coordinate $\xi = x - vt$. The equations for these waves are obtained by replacing $\partial / \partial x$ by $d / d\xi$ and $\partial / \partial t$ by $-v d / d\xi$ in (2.19)–(2.21), (2.16), (2.17). This procedure yields

$$\frac{d}{d\xi} \left[(-v + \alpha\psi + \alpha_g \psi_g) \theta + \gamma \psi_Y + \sigma\gamma\psi_g X \right] = 0, \tag{3.1}$$

$$\frac{d}{d\xi} (\psi + \beta\psi_g X) = 0, \tag{3.2}$$

$$\frac{d}{d\xi} [(1 - X)\psi_g + (\nu_g - 1)\psi_Y] = 0, \tag{3.3}$$

$$\frac{d}{d\xi} X\psi_g = \frac{w_v}{\varepsilon}, \tag{3.4}$$

$$\frac{d\psi_Y}{d\xi} = -w_r, \tag{3.5}$$

6

where we introduced notations for the fluxes of fuel, total gas and oxygen in the moving coordinate frame parameterized by ξ as

$$\psi = uf - vs, \quad \psi_g = uF_g - vS_g, \quad \psi_Y = Y(uF_g - vS_g). \tag{3.6}$$

These fluxes are functions of the dependent variables (s, X, Y, θ, u). Using (3.6), (2.18), $f_g = 1 - f$ and $s_g = 1 - s$ one can show that

$$\psi_g = \frac{u - v - uf + vs}{1 + \theta/\theta_0}. \tag{3.7}$$

We will look for a traveling wave solution, such that the temperature decreases from some value θ^- upstream ($\xi \to -\infty$) of the wave to the reservoir temperature $\theta = 0$ downstream ($\xi \to +\infty$). Also, because the rates w_r and w_v must vanish at the limiting states, we are led to the conditions at $\xi = \pm\infty$ that $s = 0$ and $X \le X_{eq}(\theta)$ or, if $s > 0$, to the conditions $Y = 0$ and $X = X_{eq}(\theta)$, see (2.27), (2.28).

We expect that the region upstream of the LTO wave contains only injected gas with a nonzero oxygen fraction, $Y > 0$. Therefore, in this region, $s = 0$. Also $X = 0$, since there is no gaseous fuel in the injected gas. Recall that dimensionless parameters are independent of u^*, so we can set its value arbitrarily. In the expression (3.6) for ψ_g, the dimensionless Darcy speed u is inversely proportional to u^*, see (2.10), (2.11); by analogy, the same is true for the dimensionless wave speed v. Thus, it is possible to choose u^* such that the gas flux is $\psi_g = 1$ in the upstream region. In summary, the following conditions for the dependent variables and fluxes must be satisfied at the limiting $(-)$ constant state

$$\begin{aligned} \xi \to -\infty: \quad & s^- = 0, \quad X^- = 0, \quad Y^- > 0, \quad \theta^- > 0, \\ & \psi^- = 0, \quad \psi_g^- = 1, \quad \psi_Y^- = Y^-, \end{aligned} \tag{3.8}$$

where the value of $\psi_Y^- = (Y\psi_g)^- = Y^-$ coincides with the oxygen fraction in the injected gas; the value of u^- is not specified.

Downstream of the LTO wave there is liquid fuel, $s > 0$, and, hence, $Y = 0$ and $X = X_{eq}(\theta)$. Thus, a limiting $(+)$ constant state is characterized by the conditions for the dependent variables and fluxes of the form

$$\begin{aligned} \xi \to +\infty: \quad & s^+ > 0, \quad X^+ = X_{eq}(0), \quad Y^+ = 0, \quad \theta^+ = 0, \\ & \psi_Y^+ = 0, \end{aligned} \tag{3.9}$$

and the value of u^+ is not specified. Having motivated (3.8) and (3.9), we will assume these boundary conditions from now on.

Algebraic equations for the wave profile can be found by integrating equations (3.1)–(3.3) from $-\infty$ to ξ, which yields

$$(-v + \alpha\psi + \alpha_g\psi_g)\theta + \gamma\psi_Y + \sigma\gamma\psi_g X = (-v + \alpha_g)\theta^- + \gamma Y^-, \tag{3.10}$$

$$\psi + \beta\psi_g X = 0, \tag{3.11}$$

$$\psi_g(1 - X) + (\nu_g - 1)\psi_Y = 1 + (\nu_g - 1)Y^-, \tag{3.12}$$

where the constants on the right-hand sides are determined using conditions (3.8) at the limiting $(-)$ state. Substituting ψ expressed from (3.11) into (3.10) yields

$$v(\theta^- - \theta) - \alpha_g(\theta^- - \psi_g\theta) - \gamma(Y^- - \psi_Y) + (\sigma\gamma - \alpha\beta\theta)\psi_g X = 0. \tag{3.13}$$

Using conditions (3.9) at the constant (+) state in (3.11)–(3.13) yields

$$\psi^+ + \beta\psi_g^+ X^+ = 0, \tag{3.14}$$

$$\psi_g^+(1 - X^+) = 1 + (\nu_g - 1)Y^-, \tag{3.15}$$

$$\sigma\gamma\psi_g^+ X^+ = (\alpha_g - v)\theta^- + \gamma Y^-, \tag{3.16}$$

where ψ^+ and ψ_g^+ denote the values computed at the (+) state.

Equations (3.14)–(3.16) are analogous to Rankine–Hugoniot relationships for shocks in conservation law theory. Given the limiting (−) state satisfying (3.8) and the wave speed v, equations (3.14)–(3.16) determine candidates for limiting (+) states satisfying (3.9). We have found the traveling wave profile once there exists a solution of equations (3.4), (3.5), (3.11)–(3.13) that connects the states (−) and (+). Such existence is the subject of the following section.

4   Traveling wave solutions

We will start the analysis by considering the case

$$\nu_g = 1, \quad \alpha = \alpha_g = \sigma = 0. \tag{4.1}$$

Typical nondimensional parameters for LTO belong to a neighborhood of these values. The value $\nu_g = 1$ corresponds to the reaction when one molecular of oxygen produces one molecular of gaseous products. According to (2.1), this can be done by taking $\nu_g = 1$. Since the fuel evaporation heat Q_v, the liquid fuel and gas sensible heats cT^* and c_gT^* are all much smaller than the combustion heat Q_r, we have $\sigma \ll 1$, $\alpha_g \ll \gamma$ and $\alpha\beta \ll \gamma$, see (2.12). Taking $\alpha = \alpha_g = \sigma = 0$, we neglect the corresponding terms in (3.13) compared to the term $\gamma(Y^- - \psi_Y)$, which is large unless $\psi_Y \approx Y^-$. The model with parameters (4.1) will be called a simplified model.

4.1   Folded surface of wave states

For the simplified model (4.1), condition (3.16) takes the form

$$\theta^- = \gamma Y^-/v. \tag{4.2}$$

It follows from (3.12) that $X \neq 1$ for parameters (4.1). Then, equations (3.11)–(3.13) become

$$f = \frac{vs}{u} - \frac{\beta X}{u(1 - X)}, \tag{4.3}$$

$$\psi_g = 1/(1 - X), \tag{4.4}$$

$$\theta = \gamma\psi_Y/v, \tag{4.5}$$

where we used (3.6) for ψ and (4.4) to obtain (4.3), and also (4.2) to obtain the last equation. Recall that the functions $\psi_g(s, \theta, u)$, $\psi_Y(s, Y, \theta, u)$ are determined in (3.6), (2.18) and the function $f(s, \theta)$ has properties (2.24)–(2.26). Using (4.3), (4.4) in (3.7), we obtain

$$u = v + \beta + \frac{1 - \beta + \theta/\theta_0}{1 - X}, \quad \text{with } \theta \text{ from (4.5)}. \tag{4.6}$$

All three terms in the right-hand side of (4.6) are positive, because $v > 0$, $\theta \geq 0$, $0 \leq X < 1$ and $0 < \beta < 1$, see (2.32). Therefore, u is positive and (4.6) implies

$$0 < v/u < 1. \tag{4.7}$$

8
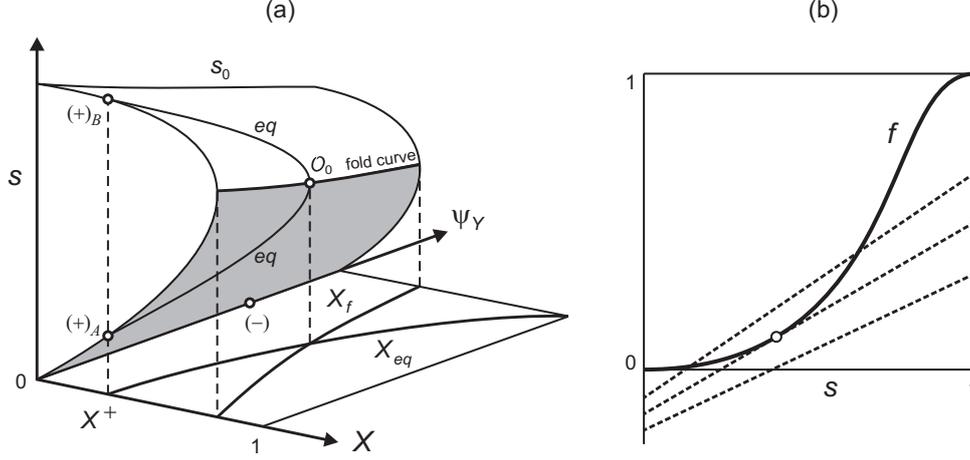
Figure 1: (a) Solutions of equation (4.3) forming a folded surface in the space (X, ψ_Y, s). The equilibrium curve $X = X_{eq}$ defined in (2.22), (4.5) determines an *eq*-curve on the surface. (b) Solutions of equation (4.3) for fixed X and ψ_Y. The left-hand side of (4.3) is represented by f in terms of s. The right-hand side as a function of s determines a straight line, whose possible positions relative to f are shown. Each point of the fold curve in figure (a) corresponds to a tangency point in (b).

Additionally, from (3.6) and (4.4), we have

$$Y = \psi_Y/\psi_g = (1 - X)\psi_Y. \tag{4.8}$$

The original state space in our problem consists of the five dependent variables (s, X, Y, θ, u), and these variables are related by equations (4.3), (4.5), (4.6). Additionally, we have the wave speed v as a parameter, which is still undetermined. Now we introduce a new state space (X, ψ_Y, s). Any point in this space determines uniquely a point in (s, X, Y, θ, u) by means of (4.8), (4.6), (4.5). In the analysis that follows, we consider (X, ψ_Y, s) as a new set of variables, which depend on the traveling coordinate ξ, constant problem parameters β, θ_0, etc., as well as on the wave speed v still to be determined. As we will see below, the remaining equation (4.3) determines a two-dimensional surface in the space (X, ψ_Y, s), where θ, u, Y are expressed in terms of X, ψ_Y using (4.5), (4.6), (4.8). The structure of the surface is described in the following proposition.

Proposition 1 *Equation (4.3) for fixed $v > 0$, with the function $f(s, \theta)$ satisfying (2.24)–(2.26), and θ, u expressed by (4.5), (4.6) determines a folded surface in the domain $0 \leq X \leq 1$, $\psi_Y \geq 0$, $0 \leq s \leq 1$, see Fig. 1(a). In the lower part of the surface $v > u\,\partial f/\partial s$, while in the upper part $v < u\,\partial f/\partial s$. The fold curve $X = X_f(\psi_Y; v)$, $s = s_f(\psi_Y; v)$ is determined by the equation*

$$v = u\,\partial f/\partial s, \tag{4.9}$$

and satisfies the inequality

$$\partial X_f/\partial \psi_Y < 0. \tag{4.10}$$

For any fixed ψ_Y, the dependence of the fold line on the parameter v is described by

$$\partial X_f/\partial v > 0, \quad \lim_{v \to 0} X_f = 0, \quad \lim_{v \to \infty} X_f = 1. \tag{4.11}$$

Proof First, let us consider an arbitrary but fixed value of $\psi_Y \geq 0$. Depending on X, equation (4.3) has a different number of solutions for s, as shown in Fig. 1(b). Here the shape

9

of the graph of f is determined by conditions (2.24)–(2.26), where θ is given by (4.5) for fixed ψ_Y. Each dashed line is the graph of the right-hand side in (4.3) as a function of s, where u is expressed by (4.6). Three lines corresponding to different parameter values are shown in Fig. 1(b). The intersection of these lines with the vertical axis $s = 0$ decreases monotonically when X increases; the intersection is at the origin for $X = 0$. The slope v/u of the dashed lines satisfies (4.7); it decreases when X increases and $v/u \to 0$ for $X \to 1$, as follows from (4.6). Using these properties, one can see that, when X is small, equation (4.3) has two solutions for s. There exists a unique $X = X_f(\psi_Y; v)$ leading to tangency, where (4.9) is satisfied, see Fig. 1(b). This tangency determines a fold shown in Fig. 1(a). For larger X, equation (4.3) has no solutions. Negative and positive signs of the quantity $v - u\,\partial f/\partial s$ for the upper and lower parts of the folded surface are recovered by inspecting the derivatives $\partial f/\partial s$ and line slopes v/u at the intersection points of the f-curve and the upper dashed line in Fig. 1(b).

Let us write (4.3) as

$$uf - vs + \beta X/(1 - X) = 0. \tag{4.12}$$

With u and θ expressed using (4.6), (4.5), equation (4.12) determines a surface in the space (X, ψ_Y, s). The normal vector (N_X, N_{ψ_Y}, N_s) to this surface is found as the gradient of the left-hand side of (4.12) as

$$N_X = \frac{f + f\theta/\theta_0 + \beta f_g}{(1 - X)^2}, \quad N_{\psi_Y} = \left(u\frac{\partial f}{\partial \theta} + \frac{f/\theta_0}{1 - X} \right) \frac{\gamma}{v}, \quad N_s = u\frac{\partial f}{\partial s} - v, \tag{4.13}$$

where $f_g = 1 - f \geq 0$. Similarly, the derivative of the left-hand side of (4.12) with respect to v is

$$N_v = -\left(u\frac{\partial f}{\partial \theta} + \frac{f/\theta_0}{1 - X} \right) \frac{\gamma Y^-}{v^2} + f - s. \tag{4.14}$$

According to (2.25), we have $\partial f/\partial \theta > 0$. Also, from (4.3), (4.7), we have $f < s$. These facts imply

$$N_X > 0, \quad N_{\psi_Y} > 0, \quad N_v < 0. \tag{4.15}$$

Let us define the fold curve by two functions, $X = X_f(\psi_Y; v)$ and $s = s_f(\psi_Y; v)$. Since $N_s = 0$ at the fold due to (4.9), we obtain

$$N_X \frac{dX_f}{d\psi_Y} + N_{\psi_Y} = 0, \tag{4.16}$$

The inequality (4.10) follows from (4.16) and (4.15). Similarly, using (4.12)–(4.14) with $N_s = 0$, we find an expression for $\partial X_f/\partial v$ as

$$N_X \frac{\partial X_f}{\partial v} + N_v = 0. \tag{4.17}$$

It follows from (4.17) and (4.15) that $\partial X_f/\partial v > 0$.

Since $u > \beta$ in (4.6), we have $v/u = 0$ in the limit $v \to 0$. In this limit equation (4.3) is satisfied only if all terms vanish, i.e., $f = X = s = 0$. As $v \to \infty$, we have the limit $X_f \to 1$. Otherwise, (4.6) yields $v/u \to 1$ and equations (4.3), (4.9) take the limiting form $f = s$, $\partial f/\partial s = 1$. But these equations have no solutions for the function f satisfying conditions (2.24)–(2.26), see Fig. 1(b). $\square$

Note that, for the simplified model (4.1), conditions (3.14), (3.15) provide two equations for the $(+)$ state and equation (3.15) yields a condition for the $(-)$ state. Thus, the $(+)$ states turn out to be independent of the $(-)$ state. Proposition 1 can be used to describe $(+)$ states of the form (3.9). There are two, one or no $(+)$ states depending on the position of the folded surface at $\psi_Y = 0$ relatively to the vertical X^+ line, see Fig. 1(a). A single $(+)$ state is found at the fold curve when $X^+ = X_f(0; v)$. Using properties (4.11), we obtain

Corollary 1 *There exists a value $v_0 > 0$ such that: there are no $(+)$ states for $v < v_0$, and there are two states $(+)_A$ and $(+)_B$ for $v > v_0$ with $s_A^+ < s_B^+$. For $v = v_0$, there is a single $(+)$ state, which lies on the fold curve.*

Thus, the case $v < v_0$ is of no interest for the study of traveling LTO waves. We assume $v \geq v_0$ from now on.

4.2 Vector field on the folded surface

We have studied equations (3.1)–(3.3) and determined the folded surface in the space (X, ψ_Y, s). Now, equations (3.4), (3.5) with ψ_g from (4.4) are written as

$$\frac{dX}{d\xi} = (1 - X)^2 \frac{w_v}{\varepsilon}, \quad \frac{d\psi_Y}{d\xi} = -w_r. \tag{4.18}$$

For given $\varepsilon > 0$, these equations define a vector field on the folded surface in Fig. 1(a). This surface can be parameterized by two coordinates (ψ_Y, s) varying in the domain

$$\psi_Y \geq 0, \quad 0 \leq s \leq s_0(\psi_Y), \tag{4.19}$$

where $s_0(\psi_Y)$ corresponds to the upper intersection of the surface with the plane $X = 0$ in Fig. 1(a). We notice that the variable $X(\psi_Y, s)$ can be expressed explicitly using (4.12) with u from (4.6) and θ from (4.5) as

$$X = \frac{v(s - f) - (1 + \theta/\theta_0)f}{v(s - f) + \beta f_g}. \tag{4.20}$$

The fold curve is defined by the condition $\partial X/\partial s = 0$.

Let us find the third component of the vector field $ds/d\xi$. Taking the derivative of (4.12) with respect to ξ and using (4.5), (4.6), (4.18) yields

$$\left(u \frac{\partial f}{\partial s} - v \right) \frac{ds}{d\xi} = \left(\frac{f/\theta_0}{1 - X} + u \frac{\partial f}{\partial \theta} \right) \frac{\gamma w_r}{v} - (f + f\theta/\theta_0 + \beta f_g) \frac{w_v}{\varepsilon}. \tag{4.21}$$

Notice that the coefficient of the left-hand side vanishes on the fold curve (4.9), giving rise to a singularity. This singularity is blown up by introducing a new coordinate τ related to ξ by the equation (a similar transformation was used in [23])

$$\frac{d\xi}{d\tau} = v - u \frac{\partial f}{\partial s}. \tag{4.22}$$

Using (4.22) in the second equation in (4.18) and (4.21), we obtain the following system, which replaces (4.18):

$$\frac{d\psi_Y}{d\tau} = \left(u \frac{\partial f}{\partial s} - v \right) w_r, \tag{4.23}$$

$$\frac{ds}{d\tau} = -\left(\frac{f/\theta_0}{1 - X} + u \frac{\partial f}{\partial \theta} \right) \frac{\gamma w_r}{v} + (f + f\theta/\theta_0 + \beta f_g) \frac{w_v}{\varepsilon}. \tag{4.24}$$

The expressions for this system contain the functions $f(s, \theta)$, $w_r(s, Y, \theta)$, $w_v(s, X, \theta)$. Using the relationships (4.20), (4.8), (4.6), (4.5), we can express the variables X, Y, u, θ and, therefore, the right-hand sides of (4.23), (4.24), as functions of the two variables ψ_Y and s.
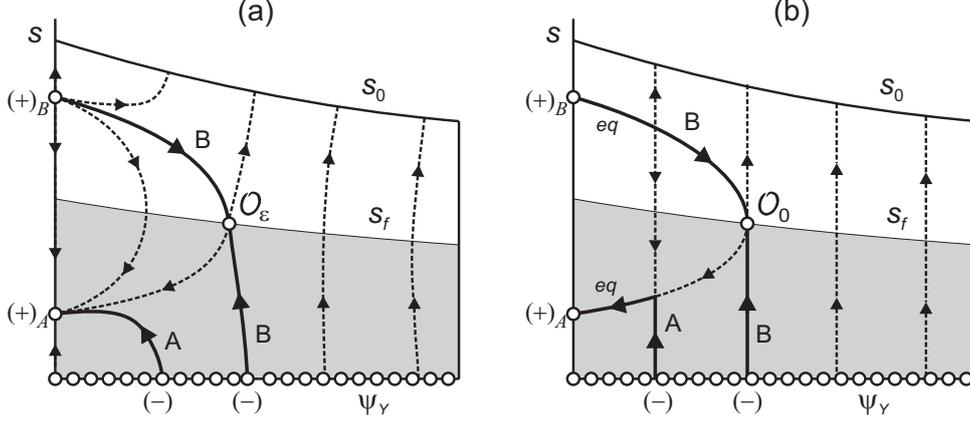
Figure 2: (a) Orbit structure of system (4.23), (4.24) for $v > v_0$ and small $\varepsilon > 0$. There is a single orbit B corresponding to a (resonant) traveling wave with the $(+)_B$ limiting state, and a family of orbits A corresponding to traveling waves with the $(+)_A$ limiting states. Arrows directions correspond to increasing τ. For increasing ξ, the arrows must be reversed in the upper (white) domain. (b) Singular limit $\varepsilon \to 0$.

Proposition 2 *Consider equilibria of system (4.23), (4.24) in the domain (4.19) for small $\varepsilon > 0$, see Fig 2. If $v > v_0$, then the equilibria on the boundary of the domain (4.19) are the two $(+)$ states and all points with $s = 0$ corresponding to $(-)$ states; there is a unique equilibrium $\mathcal{O}_\varepsilon$ in the interior of the domain (4.19). The upper $(+)_B$ state is an attractor, the lower $(+)_A$ state is a repellor, each point of the line $s = 0$ is a limiting (repelling) point of its corresponding orbit, and $\mathcal{O}_\varepsilon$ is a saddle point lying on the fold curve, see Fig 2(a). As $\varepsilon \to 0$, the point $\mathcal{O}_\varepsilon$ moves in the direction of smaller ψ_Y and has the limit $\mathcal{O}_0$. The point $\mathcal{O}_0$ is the intersection of the fold curve and the equilibrium curve marked by "eq" in Fig. 2(b); its coordinate is denoted by $\psi_Y^{(0)}$. The dependence of $\psi_Y^{(0)}$ on the parameter v is characterized by*

$$\partial \psi_Y^{(0)}/\partial v > 0, \quad \lim_{v \to v_0} \psi_Y^{(0)} = 0, \quad \lim_{v \to \infty} \psi_Y^{(0)} = \infty. \tag{4.25}$$

In the limit $v \to v_0 + 0$, the $(+)_A$, $(+)_B$ states and $\mathcal{O}_\varepsilon$ coincide.

Proof The right-hand sides of (4.23), (4.24) vanish for $s = 0$, see (2.24), (2.27), (2.28), (4.20), which also yield $X = 0$. Thus, all points with $s = 0$ are equilibria; they correspond to the $(-)$ limiting states (3.8). For small s, the w_r term in (4.24) is much smaller than the positive w_v term, as follows from the properties (2.24), (2.29), (2.30) of the functions f, w_r and w_v. Also, one can divide the right-hand sides of (4.23), (4.24) by s and obtain a vector field with regular points at $\psi_Y > 0$, $s = 0$, where $w_r = w_v = 0$. Thus, each point of the axis $s = 0$ is a limiting (repelling) point of a single corresponding orbit.

On the line $\psi_Y = 0$ we have $Y = 0$, $\theta = \gamma \psi_Y / v = 0$ and $w_r = 0$. The latter condition implies that the axis $\psi_Y = 0$ is a union of orbits of our vector field. Since the coefficient of w_v in (4.24) is positive, equilibria are determined by the condition $w_v = 0$. For $s > 0$ this implies $X = X_{eq}(0) = X^+$, determining the two $(+)$ states for $v > v_0$, see Corollary 1.

Consider the lower $(+)_A$ state with the coordinates $\psi_Y = 0$ and $s = s_A^+$. In the neighborhood of this point (4.23) yields $d\psi_Y/d\tau < 0$, since $w_r > 0$ and the coefficient in the parentheses is negative below the fold, see Proposition 1. Thus, all orbits are attracted to the axis $\psi_Y = 0$, which itself is a union of orbits, see Fig. 2(a). On the axis $\psi_Y = 0$, the sign of $ds/d\tau$ in (4.24) is determined by w_v. According to (2.29), this sign is positive for $s < s_A^+$ (when $X < X_{eq} = X^+$)

12

and negative for $s > s_A^+$ (when $X > X_{eq}$), see Fig. 1(a). Such an orbit structure for $(+)_A$ corresponds to an attractor. Similarly, one can prove that the upper $(+)_B$ state is a repellor.

Now let us consider equilibria for nonzero ψ_Y and s. In this case $w_r > 0$ as it follows from (2.27). The right-hand side of (4.23) vanishes under the condition (4.9). Therefore, equilibria lie on the fold line. Equating the right-hand side of (4.24) to zero yields

$$w_v = \varepsilon \frac{\gamma w_r}{v(1-X)} \frac{f/\theta_0 + u(1-X)\partial f/\partial \theta}{f + f\theta/\theta_0 + \beta f_g}. \tag{4.26}$$

For $\varepsilon = 0$, the solutions of (4.26) are determined by the equation $w_v = 0$. For $s > 0$, this equation yields $X = X_{eq}(\theta)$, see (2.28), and determines the eq-curve shown in Fig. 1(a). Together with the fold condition, we have $X = X_f = X_{eq}$. It follows from (2.22), (4.5) that X_{eq} increases with ψ_Y up to the value $X_{eq} = 1 > X_f$. By Proposition 1, X_f decreases with ψ_Y and, by Corollary 1, $X_f > X_{eq} = X^+$ for $\psi_Y = 0$ and $v > v_0$. Therefore, there is a unique solution with $X_f = X_{eq}$ determining the point $\mathcal{O}_0$ in Figs. 1(a) and 2(b). Since this solution is regular, it undergoes a small shift along the fold curve when ε varies from zero to a small positive value. Since the right-hand side in (4.26) is positive, we have $w_v > 0$ and (2.29) yields $X < X_{eq}$. One can see from Fig. 1(a) that the inequality $X < X_{eq}$ corresponds to the region on the right of the eq-curve in Fig. 2(b). This means that the equilibrium point $\mathcal{O}_\varepsilon$ is shifted to the positive ψ_Y-direction relative to $\mathcal{O}_0$.

Now let us study the type of the equilibrium given by equation (4.26) for $\varepsilon > 0$ and the fold condition (4.9). At the fold we have $\partial X/\partial s = 0$. This allows writing the Jacobian of the right-hand side of system (4.23), (4.24) at the equilibrium as

$$\begin{pmatrix} * & uw_r \dfrac{\partial^2 f}{\partial s^2} \\ \dfrac{f + f\theta/\theta_0 + \beta f_g}{\varepsilon} \dfrac{\partial w_v}{\partial \theta} \dfrac{\gamma}{v} + * & * \end{pmatrix}, \tag{4.27}$$

where we used $\partial\theta/\partial\psi_Y = \gamma/v$, which follows from (4.5); the stars denote terms which have finite limit as $\varepsilon \to 0$. The upper right component is positive, since $\partial^2 f/\partial s^2 > 0$ at the fold corresponding to the tangency in Fig. 1(b). The derivative $\partial w_v/\partial\theta$ is positive, which can be shown by differentiating the equality $w_v(s, X_{eq}(\theta), \theta) = 0$ with $\partial w_v/\partial X < 0$ and $\partial X_{eq}/\partial\theta > 0$, see (2.28), (2.22). Thus, the lower left component is positive. For sufficiently small ε, when the $1/\varepsilon$ term is much larger than the other terms, the determinant of (4.27) is negative. Hence, the equilibrium is a saddle with eigenvectors almost parallel to the s-axis, as one can check by evaluating eigenvalues and eigenvectors of (4.27).

As we showed above, the coordinate $\psi_Y^{(0)}(v)$ of the point $\mathcal{O}_0$ is determined by the equations $X = X_f(\psi_Y; v) = X_{eq}(\theta)$, where $\theta = \gamma\psi_Y/v$. It is straightforward to show $d\psi_Y^{(0)}/dv > 0$ by differentiating the equation $X_f = X_{eq}$ and using the inequalities $\partial X_f/\partial\psi_Y < 0$, $\partial X_f/\partial v > 0$ and $dX_{eq}/d\theta > 0$, see (4.10), (4.11) and (2.22). In the limit $v \to \infty$, we have $X_{eq} = X_f \to 1$ according to (4.11), which implies $\theta \to 1$, see (2.22). Using (4.5), this yields $\psi_Y^{(0)} \to \infty$ as $v \to \infty$. By Corollary 1, for $v = v_0$, the $(+)_A$ and $(+)_B$ states coincide at the point where $X = X_f = X_{eq}$, see Fig. 1(a). At this point, equation (4.26) is satisfied for any ε and, therefore, all three equilibria $(+)_A$, $(+)_B$ and $\mathcal{O}_\varepsilon$ merge. In particular, we have $\psi_Y^{(0)}(v_0) = 0$. $\square$

For numerical aspects of finding the LTO wave parameters see Section 6.

4.3   Non-resonant and resonant waves

For fixed small $\varepsilon > 0$ and $v > v_0$, the qualitative orbit structure is presented in Fig. 2(a). This orbit structure is fully determined by the equilibria described in Proposition 2. Note that for

$\psi_Y > 0$ the orbit directions are characterized by $d\psi_Y/d\tau > 0$ above the fold and $d\psi_Y/d\tau < 0$ below the fold, see (4.23) and Proposition 1.

A traveling wave is represented by an orbit of (4.23), (4.24) on the plane (ψ_Y, s) starting at a $(-)$ state on the axis $s = 0$ and ending at a $(+)$ state on the axis $\psi_Y = 0$. The traveling coordinate ξ must increase along the orbit from $(-)$ to $(+)$. It follows from (4.22) and Proposition 1 that the coordinate τ must increase along the orbit below the fold (grey regions in Figs. 1, 2) and decrease above the fold (white regions). Note that the fold states given by (4.9) are resonant states, because $u\,\partial f/\partial s$ is the saturation characteristic speed. We will say that the wave is *resonant* if it contains a resonance state, i.e., the corresponding orbit passes through the fold.

One can see that there exist two types of traveling waves in our problem. The first type corresponds to the resonant wave. The resonant wave profile is represented by an orbit that crosses the fold and is denoted by B in Fig. 2. This orbit connects the state $(-)$ given by $\psi_Y = Y^-$, $s = 0$ to the state $(+)_B$ given by $\psi_Y = 0$, $s = s_B^+$, see (3.8), (3.9). Note that the orbit must pass through the saddle equilibrium, since the condition of increasing ξ cannot be satisfied at a regular point on the fold. (Recall that ξ increases with τ below the fold, and decreases with τ above the fold.) Though $\tau \to \infty$ at the equilibrium, one can show that ξ remains finite, since the right-hand side in (4.22) vanishes on the fold. One can see that the orbit B exists only for the specific value of $Y^- = Y_B$.

The second type corresponds to non-resonant waves. Their profiles are represented by orbits that lie below the fold and are denoted by A in Fig. 2. Such orbits connect states $(-)$ given by $\psi_Y = Y^-$, $s = 0$ to the state $(+)_A$, see Fig. 1(a). The orbits A exist for $Y^- \le Y_B$, where Y_B corresponds to the $(-)$ state of the orbit B, see Fig. 2.

The structure of orbits of system (4.23), (4.24) in the limit $\varepsilon \to 0$ is shown in Fig. 2(b). Rescaling $\tau = \varepsilon\tilde{\tau}$ and taking $\varepsilon = 0$ in this system yields $d\psi_Y/d\tilde{\tau} = 0$ and $ds/d\tilde{\tau} = (f + f\theta/\theta_0 + \beta f_g)w_v$. A set of equilibria of this system is determined by the condition $w_v = 0$ and consists of the line $s = 0$ and the *eq*-curve. Away from this set, all orbits are parallel to the s-axis. The directions of these orbits are determined by the sign of w_v according to (2.29). This sign is negative for $X > X_{eq}$ (on the left of the *eq*-curve), and positive for $X < X_{eq}$ (on the right of the *eq*-curve), see Fig. 1(a). The *eq*-curve represents a limit of two saddle orbits, see Fig. 2(a,b).

We see that the classification of traveling waves for a given speed $v > v_0$ is determined by the value of Y_B. In the limit $\varepsilon \to 0$, we have $Y_B = \psi_Y^{(0)}$, since the orbit B is parallel to the s-axis below the equilibrium $\mathcal{O}_0$ with the abscissa $\psi_Y^{(0)}$, see Fig. 2(b). Hence, $dY_B/dv = d\psi_Y^{(0)}/dv > 0$, see (4.25). For small positive ε, the difference between Y_B and $\psi_Y^{(0)}$ is small and, thus, the inequality $dY_B/dv > 0$ remains valid. This allows associating a unique value $v = v_r$ for given $Y_B > 0$ and small fixed $\varepsilon > 0$. In this case, the family of non-resonant traveling waves for given Y^- is characterized by speeds $v \ge v_r$ (instead of $Y^- \le Y_B$ for given v).

The results we obtained can be summarized as follows.

Theorem 1 *Consider system (2.13)–(2.17) for the simplified model with parameters (4.1), small $\varepsilon > 0$, and oxygen fraction $0 \le Y^- \le 1$ in the injected gas. Then there exists a critical speed value $v_r > 0$ such that:*

1) *For any $v \ge v_r$, there exists a non-resonant traveling wave with speed v and with limiting states satisfying (3.8), (3.9), where $\theta^- = \gamma Y^-/v$ and $s^+ = s_A^+$ at $(+)_A$ in Fig. 2(a). At the $(+)_A$ state, the inequality $v > u\,\partial f/\partial s$ holds.*

2) *There exists a unique resonant traveling wave with limiting states satisfying (3.8), (3.9). This wave has speed $v = v_r$. The limiting values are $\theta^- = \gamma Y^-/v_r$ and $s^+ = s_B^+$ at $(+)_B$ in Fig. 2(a). At the $(+)_B$ state, the inequality $v < u\,\partial f/\partial s$ holds.*

3) *If $v < v_r$, then traveling waves with limiting states satisfying (3.8), (3.9) do not exist.*
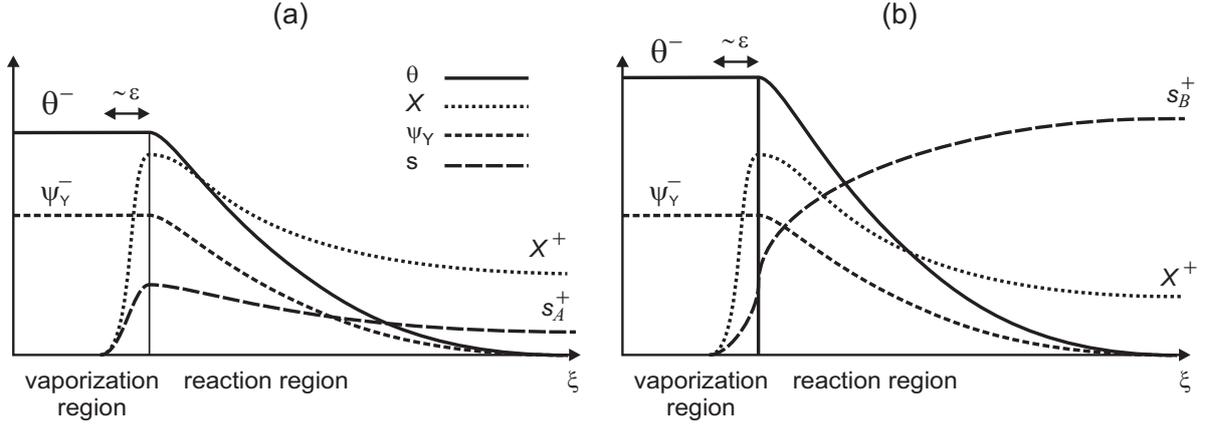
Figure 3: Structure of non-resonant (a) and resonant (b) LTO waves for the simplified model
(4.1). Indicated are changes in temperature θ, liquid fuel saturation s, oxygen flux ψ_Y and
fuel fraction X in the gas. One region is dominated by vaporization and the other by LTO
reaction (with slow condensation). In case (b), these regions are separated by the resonance
state corresponding to $\mathcal{O}_\varepsilon$ in Fig. 2(a). The reaction region is much wider than the vaporization
region. The variations of θ and ψ_Y in the vaporization region are small (of order ε) for parameters
(4.1).

*In the limit $\varepsilon \to 0$, the speed v_r can be found by solving equations (4.3), (4.9) with respect to v
and s, where $X = X_{eq}(\theta)$, $\psi_Y = Y^-$ and θ, u are taken from (4.5), (4.6).*

In practical applications, ε is usually very small, and it is sufficient to use the approximation
with $\varepsilon \to 0$. According to Theorem 1, the classification of the LTO traveling waves in this limit
requires solving a system of two algebraic equations. These equations depend on the values of
the constant parameters Y^-, γ, β, θ_0, θ_v, as well as on the form of the function $f(s, \theta)$.

Fig. 3 shows profiles of non-resonant and resonant LTO waves corresponding to the orbits
A and the orbit B respectively in Fig. 2. One can distinguish two regions in the profile. In the
vaporization region upstream of the wave, the gaseous fuel fraction increases from $X = 0$ in the
injected air to its equilibrium profile $X_{eq}(\theta)$. Due to large vaporization rate ($\varepsilon \ll 1$), this region
is very thin so that the total amounts of reaction products are small. The second much wider
reaction region is where almost all of the LTO reaction occurs. In this region, the fraction X
remains very close to $X_{eq}(\theta)$. The decrease of X with ξ implies that condensation of gaseous fuel
occurs in the reaction region. This condensation is characterized by a much smaller vaporization
rate $|w_v|$ compared to the rate in the vaporization region. In the resonant wave, the subdivision
into vaporization and reaction regions may be attributed to the saddle equilibrium, as one can
conclude looking at the position of the orbit B and the *eq*-curve in Fig. 2(b). See also the profile
of the resonant LTO wave computed numerically in Section 6 and presented in Fig. 5(b), where
the thin vaporization region is shown as a discontinuity.

4.4 Generalization

The results obtained above correspond to the system (3.1)–(3.5) simplified by taking parameters
(4.1). As shown above, values of parameters corresponding to physical systems can be considered
as small perturbations of (4.1). In the general case, equations (3.11)–(3.13) with (3.16) and ψ

from (3.6) yield

$$f = \frac{vs}{u} - \frac{\beta\psi_g X}{u}, \tag{4.28}$$

$$\psi_g = \frac{1 + (\nu_g - 1)(Y^- - \psi_Y)}{1 - X}, \tag{4.29}$$

$$\theta = \frac{\gamma\psi_Y + \sigma\gamma(\psi_g X - \psi_g^+ X^+)}{v + (\alpha\beta X - \alpha_g)\psi_g}. \tag{4.30}$$

Using (4.28) in (3.7), we obtain

$$u = v + \psi_g(1 - \beta X + \theta/\theta_0). \tag{4.31}$$

Equations (4.28)–(4.31) substitute (4.3)–(4.6). The first equation (4.28) with ψ_g, θ, u expressed from (4.29)–(4.31) defines a surface in the space (X, ψ_Y, s). It is clear that, for parameters taken in a neighborhood of (4.1), this surface has the same folded structure described in Proposition 1 and shown in Fig. 1(a). In particular, the fold condition takes the same form (4.9), but with u given by (4.31). Traveling waves are described as orbits of the system induced by equations (3.4), (3.5) on the folded surface.

The structure of orbits again can be studied using the (ψ_Y, s) projection of the folded surface. Following the derivation of (4.22)–(4.24), one can check that the first two equations remain unchanged in the general case. In the last equation, only the coefficients of w_r and w_v on the right-hand side will change. Thus, for parameters taken in a neighborhood of (4.1), Proposition 2 can be proved as in the simplified case.

The following theorem provides an extension of Theorem 1.

Theorem 2 *The traveling wave classification of Theorem 1 holds when the parameters ν_g, α, α_g, σ are taken in some neighborhood of (4.1). In the limit $\varepsilon \to 0$, the critical value $v = v_r$ can be found by solving equations (4.3), (4.9), $X = X_{eq}(\theta)$ with respect to v, X, s, where $\psi_Y = Y^-$, u is given by (4.6), and*

$$\theta^- = \frac{\gamma Y^-}{v - \alpha_g} - \frac{\sigma\gamma(1 + (\nu_g - 1)Y^-)X^+}{(v - \alpha_g)(1 - X^+)}, \quad \theta = \frac{(v - \alpha_g)(1 - X)\theta^- + \sigma\gamma X}{v(1 - X) - \alpha_g + \alpha\beta X}. \tag{4.32}$$

Proof The proof of Theorem 1 was based on Propositions 1, 2, which are valid also in a neighborhood of the parameters in (4.1). Thus, the classification of traveling waves in Theorem 1 remains valid. In the limit $\varepsilon \to 0$, the same conditions (4.9), $X = X_{eq}(\theta)$, $\psi_Y = Y^-$ hold at the resonance point. Substituting the latter into (4.28), (4.29), (4.31) yields equations (4.3), (4.4), (4.6) at the resonance point. The first expression in (4.32) is obtained from (3.16), where ψ_g^+ is expressed from (3.15). Then the second expression in (4.32) is derived from (3.13), where $\psi_Y = Y^-$ and ψ_g is expressed from (4.4). $\square$

As described in Theorems 1 and 2, in the limit $\varepsilon \to 0$, the speed v_r of the resonant wave is determined by the conditions $X = X_{eq}(\theta)$, $\psi_Y = Y^-$ at the resonance point. Thus, the speed v_r becomes independent of the particular form of the reaction and vaporization rates w_r, w_v. We also note that, in the general case, the temperature profile $\theta(\xi)$ will not be monotonic as in Fig. 3, but will have a (usually small) increasing part in the vaporization region.

4.5 Equations structure and the resonance

Let us give some general remarks about the governing system (2.19)–(2.21), (2.16), (2.17), which has the structure

$$\frac{\partial H}{\partial t} + \frac{\partial F}{\partial x} = G, \tag{4.33}$$

16

where $H, F, G \in \mathbb{R}^5$ are smooth functions of the dependent variables $U = (s, X, Y, \theta, u)$. Limiting states of the traveling wave must satisfy the condition $G = 0$.

For a traveling wave, equation (4.33) yields

$$D\frac{\partial U}{\partial \xi} = G, \quad D = -v\frac{\partial H}{\partial U} + \frac{\partial F}{\partial U}, \tag{4.34}$$

where $\xi = x - vt$ is the traveling coordinate and v is the wave speed. This is a system of implicit ordinary differential equations. In the generic case, the state space U can be divided into a set of open connected regions with boundaries. In the interior of each region, the matrix D is nonsingular, so that (4.34) yields a differential equation for the wave profile as $dU/d\xi = D^{-1}G$. The regions are separated by hypersurfaces with singular matrices D. Thus, when the limiting states of the wave belong to different regions, the wave profile must contain an intermediate state with singular matrix D. This state is resonant, since the equation $\det D = 0$ for the matrix D from (4.34) implies that v is a characteristic speed of system (4.33).

In our problem, (4.34) represents a system of five equations. The first three components of G are identically zero, which allows integration of the first three equations. This yields explicit expressions for θ and u, as well as a folded surface in the space (X, Y, s) or, after a simple transformation, in the space (X, ψ_Y, s). The remaining two equations of system (4.34) define the vector field on the folded surface, where the fold corresponds to the boundary $\det D = 0$ discussed in the previous paragraph. We have seen that the orbit of the vector field (corresponding to a traveling wave) can pass only through a singular point of the fold. Note that the singularity that we encountered on the fold line can be seen as a typical folded saddle singularity of a system of two implicit ordinary differential equations, see [1, 5].

We see that singularities of implicit ordinary differential equations are strongly related to the problem of finding traveling wave profiles in systems of balance laws (4.33). It was mentioned in [12] that, besides the Rankine-Hugoniot conditions relating $(-)$ and $(+)$ limiting states, analysis of the singularity at the resonance point $\mathcal{O}_\varepsilon$ provides extra determining conditions. Physical examples of this phenomenon are encountered in detonation problems [23, 6, 11], where it is called "pathological detonation". We identified and studied this singularity in our problem of low temperature oxidation in porous medium, and showed that it joins the vaporization and reaction regions. The novel part of our theory is related to the limit $\varepsilon \to 0$, corresponding to large vaporization rate. In this limit, the extra determining condition becomes independent of the form of both the vaporization and reaction rates, i.e., of the function G in (4.33); only the Clausius-Clapeyron relation (2.9) remains important. The limiting extra condition is found explicitly; it determines the LTO wave speed for given injection conditions. We hope that our approach can be used to yield rigorous results in the opposite case of large reaction rate, e.g., in the problem of detonation in slightly divergent flow [6].

5   Wave sequence solutions

The singular structure of the LTO wave has interesting consequences for a general solution. To see this, let us return to the original system (2.13)–(2.17) and consider the large time asymptotic behavior. At large spacial and temporal scales, the LTO wave can be treated as a discontinuity between the limiting states (3.8), (3.9). In this case we can construct a general solution as a sequence of waves, such that all waves are well separated in space and do not interact. For simplicity, we will stick to the case (4.1).

Upstream of the LTO wave, there is no fuel and $s = X = w_r = w_e = 0$. To model air injection, we prescribe the boundary condition as

$$x = 0: \quad \theta = s = X = 0, \quad Y = Y_{inj}, \quad u = u_{inj}, \tag{5.1}$$

where Y_{inj} is the oxygen fraction in injected gas, and u_{inj} describes the injection rate. The far downstream state corresponds to the prescribed initial reservoir filled with liquid fuel with saturation s_{res} and gas with saturation $1 - s_{res}$. This gas contains fuel vapor and no oxygen. Thus,

$$x \to \infty: \quad \theta = 0, \quad s = s_{res}, \quad X = X_{eq}(0), \quad Y = 0. \tag{5.2}$$

Let us study the behavior near the injection point. In this region, $s = X = w_r = w_e = 0$ and $Y \equiv Y_{inj}$. Hence, equations (2.14), (2.16) are trivially satisfied and (2.17) is equivalent to (2.15). Using (2.18), the remaining equations (2.13), (2.15) reduce to

$$\frac{\partial \theta}{\partial t} = 0, \quad \frac{\partial}{\partial t} \frac{1}{1 + \theta/\theta_0} + \frac{\partial}{\partial x} \frac{u}{1 + \theta/\theta_0} = 0. \tag{5.3}$$

These equations have a shock wave solution (thermal wave) described as a discontinuity at $x = v_T t$ between the injection state (5.1) and the LTO wave $(-)$ state (3.8). Using the Rankine–Hugoniot conditions on these states for (5.3) (see, e.g., [20]), we obtain

$$v_T[\theta] = 0, \quad \left[\frac{u - v_T}{1 + \theta/\theta_0}\right] = 0, \tag{5.4}$$

with the braces denoting the variation of the expression at the discontinuity. This yields

$$v_T = 0, \quad u^- = (1 + \theta^-/\theta_0)u_{inj}. \tag{5.5}$$

Note that the vanishing speed is the result of (4.1); v_T becomes positive for $a_g > 0$ (for typical parameters the thermal wave is much slower than the LTO wave). The thermal wave is the only wave that can be found upstream of the LTO wave. This implies that

$$Y^- = Y_{inj}. \tag{5.6}$$

First let us consider the resonant LTO wave as a discontinuity at $x = vt$ between the limiting states (3.8), (3.9). Equation (4.3) for the $(+)$ state (3.9) has two solutions s_A^+ and s_B^+, Fig. 4. By Theorem 1, the resonant wave is characterized by the specific speed value $v = v_r$ and the larger saturation s_B^+. Recall that the reference speed u^* must be chosen so that $\psi_g^- = 1$, see (3.8). Expressing ψ_g^- from (3.6), (2.18) and using (5.5), $s^- = f^- = 0$, and θ^- from (4.2), we obtain

$$u_{inj} = 1 + \frac{v_r^2}{v_r + \gamma Y^-/\theta_0}. \tag{5.7}$$

This formula can be used to find the relation v_r/u_{inj} between the LTO wave speed and the injection speed.

Consider now the region downstream of the LTO wave, where $\theta^+ = Y^+ = w_r^+ = w_v^+ = 0$ and X^+ are constant, see (3.9). For $\theta = Y = w_r = w_v = 0$, equations (2.13), (2.17) are trivially satisfied, and equations (2.14)–(2.16) are equivalent to

$$\frac{\partial s}{\partial t} + \frac{\partial F}{\partial x} = 0, \tag{5.8}$$

where the flux function $F(s) = u^+ f(s, 0)$ corresponds to the $(+)$ state with $u = u^+$ and $\theta^+ = 0$. A self-similar weak solution (saturation wave) has the form $s = s(\zeta)$ with $\zeta = x/t$. This solution is constructed using the standard procedure, see, e.g., [17, 20]. Generally, it represents a shock or rarefaction waves, possibly combined. The states $s(\zeta)$ in this solution are found by taking the convex hull of the portion of graph of the function $F(s)$ between the limiting points s_B^+ and s_{res} with increasing slope ζ. The lower part of the convex hull is taken when $s_B^+ < s_{res}$, and the upper part when $s_B^+ < s_{res}$. Examples of saturation wave solutions are shown in Fig. 4.
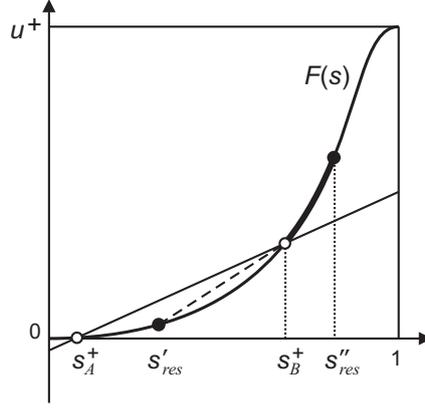
Figure 4: Presented are the function $F(s) = u^+ f(s, 0)$ and the straight line with slope v_r and intersection with the vertical axis at $-\beta X^+/(1 - X^+)$. The downstream fuel saturation s_B^+ of the resonant LTO wave corresponds to the upper intersection point. Downstream fuel saturations of non-resonant LTO waves span the interval $(0, s_A^+]$ below the lower intersection point. As examples, two dark points determine the values of s_{res} connected to s_B^+ by a saturation wave. It is a shock wave (dashed line) for the lower point denoted as s_{res}', and a rarefaction wave (bold line) for the upper point denoted as s_{res}''.

We must have $\zeta \geq v_r$ in the saturation wave, since the saturation wave must be downstream of the LTO wave. One can see from Fig. 4 that solutions $s(\zeta)$ satisfying this requirement exist when $s_{res} \geq s_A^+$, where s_A^+ is the lower intersection point.

When $s_{res} < s_A^+$, solutions with a resonant LTO wave do not exist. In this case, the solutions can be constructed with non-resonant LTO waves. According to Theorem 1, non-resonant waves exist for $v \geq v_r$. With increasing v, the value of s_A^+ decreases and vanishes in the limit $v \to \infty$. This can be seen from Fig. 1(b), taking into account that, for $v \to \infty$, the line slope v/u^+ tends to 1 and the intersection point of the line with the vertical axis tends to the origin, see (4.3), (4.6). Since non-resonant waves satisfy the condition $v > u \, \partial f/\partial u$, there cannot be a saturation wave downstream. We summarize the results in

Theorem 3 *Consider the system (2.13)–(2.17) with parameters (4.1), small $\varepsilon > 0$, and oxygen fraction $0 < Y^- \leq 1$ in the injected gas. Let s_A^+ be the value at the $(+)_A$ limiting state (3.9) computed for the speed $v = v_r$ according to Corollary 1 and Theorem 1. Then,*

1) *If $s_{res} \geq s_A^+$, there is a unique asymptotic solution as a sequence of thermal, resonant LTO and saturation waves, separating the four regions with constant states (5.1), (3.8), (3.9), (5.2). When $s_{res} = s_A^+$, the LTO wave speed is equal to the speed of the saturation (shock) wave.*

2) *If $s_{res} \leq s_A^+$, there is a unique asymptotic solution as a sequence of thermal and non-resonant LTO waves separating the three regions with constant states (5.1), (3.8), (5.2).*

The saturation wave in case 1 of Theorem 3 can be a rarefaction or a shock (possibly combined) as explained in Fig. 4. Note the remarkable role of the resonant LTO wave, which appears in the solution for a wide range of the initial fuel concentrations $s_{res} \geq s_A^+$.

6   Numerical example

Let us consider the simplified case (4.1) with other parameters and viscosity ratio given by

$$\gamma = 0.14, \quad \beta = 0.05, \quad \theta_0 = 2, \quad \theta_v = 25, \quad \mu_g/\mu = 0.04(1 + 1.2\,\theta)\sqrt{\theta + 2.2}, \qquad (6.1)$$
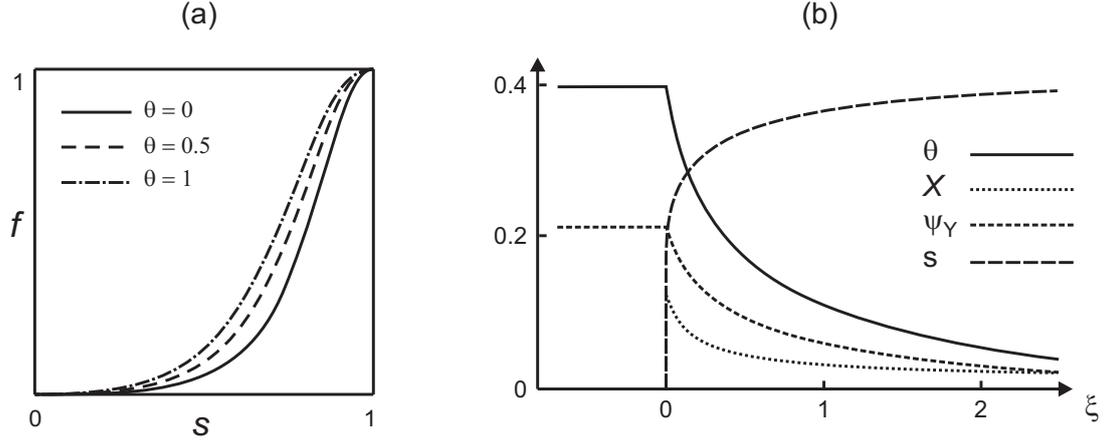
Figure 5: (a) Fractional flow function $f(s,\theta)$ for different θ. (b) Resonant LTO wave profile in the limit $\varepsilon \to 0$ for $Y_{inj} = 0.21$ and reaction rate (6.2). The vaporization region reduces to a discontinuity of s and X at $\xi = 0$. The reaction region corresponds to $\xi > 0$.

typical for a light oil reservoir ($P_{tot} = 10\,\text{atm}$, $T_{res} = 50°\text{C}$, $T_b = 200°\text{C}$, etc.). We will consider the limit $\varepsilon \to 0$, since ε is usually extremely small. The quadratic permeability Corey model with $k = s^2$, $k_g = s_g^2$ will be used. Graphs of the fractional flow function $f(s,\theta)$ determined in (2.7) are presented in Fig. 5(a) for different values of θ.

Consider the injected oxygen fraction $Y^- = Y_{inj} = 0.21$. By Theorem 1, the resonant LTO wave speed v_r together with the fuel saturation s at the resonance point are found by solving numerically equations (4.3), (4.9) with $X = X_{eq}(\theta)$ in (2.22), $\psi_Y = Y^-$ and θ, u from (4.5), (4.6). Solving these equations numerically, we find $v_r = 0.0743$. Solving equation (4.3) for the (+) state (3.9), we find the larger solution $s_B^+ = 0.4060$ corresponding to the resonant LTO wave, and the smaller solution $s_A^+ = 0.0107$. Since s_A^+ is very small, for almost all initial fuel saturations ($s_{res} > s_A^+$), the wave sequence solution contains a resonant LTO wave.

The wave profile of the resonant LTO wave consists of vaporization and reaction regions, see Fig. 3(b). As $\varepsilon \to 0$, the vaporization region reduces to a discontinuity in the upstream part of the profile. In the reaction region, we can express θ, $X = X_{eq}(\theta)$, u, Y in terms of ψ_Y using (4.5), (4.6) and (4.8). Then s as a function of ψ_Y is determined by the larger solution of (4.3); it corresponds to the orbit B above the equilibrium $\mathcal{O}_0$ in Fig. 2(b). When the expression for w_r is known, one can use these relations for finding the spatial dependence $\psi_Y(\xi)$ by integrating numerically the differential equation (3.5) with the initial condition $\psi_Y(0) = Y_{inj}$ at the equilibrium $\mathcal{O}_0$. Let us consider an LTO reaction rate of the form

$$w_r = 10^9 s Y^{0.5} \exp\left(-\frac{45}{\theta_0 + \theta}\right), \tag{6.2}$$

which agrees with experimental data in [7]. For this case, the profile of the resonant LTO wave is shown in Fig. 5(b).

Instead of (4.1), we also considered the parameters

$$\nu_g = 0.5, \quad \alpha = 0.23, \quad \alpha_g = 0.0016, \quad \sigma = 0.08. \tag{6.3}$$

In this case the resonant LTO wave speed $v_r = 0.0766$ is computed numerically as described in Theorem 2. The calculations show that the results for the cases (4.1) and (6.3) are very close. Numerical computations confirmed the existence and uniqueness of the traveling wave profile for the resonant LTO wave, as predicted by Theorem 2.

20

7 Conclusion

We studied traveling waves in reactive multi-phase flow in porous medium described by a system of conservation laws with two source terms corresponding to oxidation and vaporization. We identified and studied traveling waves that contain resonance points, at which the wave speed equals the saturation characteristic speed. The wave profile is determined as an orbit of a vector field in state space. The resonance point is associated to a saddle singularity of this vector field defined on a folded surface. This folded saddle singularity leads to an extra condition relating the states upstream and downstream of the traveling wave. It is remarkable that this condition does not depend on the form of reaction and vaporization rates, provided one of the processes (in our case vaporization) is much faster than the other. In this limit, the extra determining condition was found explicitly. We proved existence and uniqueness theorems for resonant waves, and found general solutions of the problem in the form of wave sequence. We showed that the wave sequence solution for physically relevant initial conditions contains the resonant traveling wave.

Singularities at internal points of traveling wave profiles are shown to play important role in filtration combustion problems, which motivates further study of such singularities. This theory would be useful, e.g., when an extra liquid phase (such as water) is taken into account. In our model we neglected parabolic terms, e.g., from heat conduction, whose effect onto the qualitative structure of the traveling wave solution needs to be studied. All these problems are important both for the mathematical theory of PDEs and for flow in porous media.

References

[1] D. V. Anosov and V. I. Arnold. Dynamical Systems. I. Ordinary Differential Equations and Smooth Dynamical Systems, 1988.

[2] A. Bayliss and B. J. Matkowsky. From traveling waves to chaos in combustion. *SIAM J. Appl. Math.*, 54:147–174, 1994.

[3] P. Bedrikovetsky and G. Rowan. *Mathematical Theory of Oil and Gas Recovery: with Applications to Ex-USSR Oil and Gas Fields.* Kluwer, 1993.

[4] J. Bruining, A. A. Mailybaev, and D. Marchesin. Filtration combustion in wet porous medium. *SIAM J. Appl. Math.*, 70:1157–1177, 2009.

[5] A. A. Davydov. Normal forms of differential equations unresolved with respect to derivatives in a neighbourhood of its singular point. *Funct. Anal. Appl.*, 19:1–10, 1985.

[6] W. Fickett and W. C. Davis. *Detonation: Theory and Experiment.* Dover, Mineola, N.Y., 2011.

[7] N. P. Freitag and B. Verkoczy. Low-temperature oxidation of oils in terms of SARA fractions: why simple reaction models don't work. *Journal of Canadian Petroleum Technology*, 44(3):54–61, 2005.

[8] D. Gutierrez, A. Taylor, V. Kumar, M. Ursenbach, R. Moore, and S. Mehta. Recovery factors in high-pressure air injection projects revisited. *SPE Reservoir Evaluation & Engineering*, 11(6):1097–1106, 2008.

[9] J. Härterich and S. Liebscher. Travelling waves in systems of hyperbolic balance laws. *In: G. Warnecke, Ed., Analysis and Numerical Methods for Conservation Laws. Springer-Verlag, 2005.*

[10] E. Isaacson, D. Marchesin, B. V. Plohr, and J. B. Temple. Multiphase flow models with singular Riemann problems. *Mat. Aplic. Comp.*, 1992.

[11] A. G. Kulikovskii and N. T. Pashchenko. Propagation regimes of self-supported light-detonation waves. *Fluid Dynamics*, 40(5):818–828, 2005.

[12] A. G. Kulikovskii, N. V. Pogorelov, and A. Y. Semenov. *Mathematical Aspects of Numerical Solution of Hyperbolic Systems.* Chapman and Hall/CRC, Boca Raton, FL, 2001.

[13] A. A. Mailybaev, J. Bruining, and D. Marchesin. Analysis of in situ combustion of oil with pyrolysis and vaporization. *Combustion and Flame*, 158(6):1097–1108, 2011.

[14] A. A. Mailybaev, J. Bruining, and D. Marchesin. Interaction of combustion and evaporation in low temperature oxidation of light oil. 2011. In preparation.

[15] D. Marchesin and A. A. Mailybaev. Dual-family viscous shock waves in n conservation laws with application to multi-phase flow in porous media. *Archive for Rational Mechanics and Analysis*, 182(1):1–24, 2006.

[16] B. J. Matkowsky and G. Sivashinsky. Propagation of a pulsating reaction front in solid fuel combustion. *SIAM J. Appl. Math.*, 35:465–478, 1978.

[17] O. A. Oleinik. Construction of a generalized solution of the Cauchy problem for a quasilinear equation of first order by the introduction of vanishing viscosity. *Uspekhi Matematicheskikh Nauk*, 14(2):159–164, 1959.

[18] D. A. Schult, B. J. Matkowsky, V. A. Volpert, and A. C. Fernandez-Pello. Forced forward smolder combustion. *Combustion and Flame*, 104:1–26, 1996.

[19] G. J. Sharpe and S. Falle. One-dimensional nonlinear stability of pathological detonations. *Journal of Fluid Mechanics*, 414(1):339–366, 2000.

[20] J. Smoller. *Shock Waves and Reaction-Diffusion Equations.* Springer, New York, 1983.

[21] C. W. Wahle, B. J. Matkowsky, and A. P. Aldushin. Effects of gas-solid nonequilibrium in filtration combustion. *Combust. Sci. and Tech.*, 175:1389–1499, 2003.

[22] S. Whitaker. Simultaneous heat, mass and momentum transfer in porous media: a theory of drying. *Advances in Heat Transfer*, 13(1):19–203, 1977.

[23] W. W. Wood and Z. W. Salsburg. Analysis of steady-state supported one-dimensional detonations and shocks. *Physics of Fluids*, 3:549–566, 1960.

[24] Z. Xu, L. Jianyi, S. Liangtian, L. Shilun, and L. Weihua. Research on the mechanisms of enhancing recovery of light-oil reservoir by air-injected low-temperature oxidation technique. *Natural Gas Industry*, 24:78–80, 2004.

[25] Y. B. Zeldovich, G. I. Barenblatt, V. B. Librovich, and G. M. Makhviladze. *The Mathematical Theory of Combustion and Explosion.* Consultants Bureau, New York, 1985.